NANO LETTERS

pubs.acs.org/NanoLett Letter

Wafer-Scale Highly Oriented Monolayer MoS_2 with Large Domain Sizes

Qinqin Wang, Na Li, Jian Tang, Jianqi Zhu, Qinghua Zhang, Qi Jia, Ying Lu, Zheng Wei, Hua Yu, Yanchong Zhao, Yutuo Guo, Lin Gu, Gang Sun, Wei Yang, Rong Yang, Dongxia Shi, and Guangyu Zhang*

Cite This: https://dx.doi.org/10.1021/acs.nanolett.0c02531 Read Online

ACCESS | Metrics & More | Article Recommendations | Supporting Information

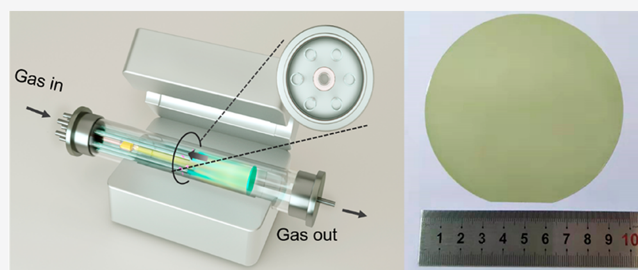

ABSTRACT: Two-dimensional molybdenum disulfide (MoS_2) is an emergent semiconductor with great potential in next-generation scaled-up electronics, but the production of high-quality monolayer MoS_2 wafers still remains a challenge. Here, we report an epitaxy route toward 4 in. monolayer MoS_2 wafers with highly oriented and large domains on sapphire. Benefiting from a multisource design for our chemical vapor deposition setup and the optimization of the growth process, we successfully realized material uniformity across the entire 4 in. wafer and greater than 100 μm domain size on average. These monolayers exhibit the best electronic quality ever reported, as evidenced from our spectroscopic and transport characterizations. Our work moves a step closer to practical applications of monolayer MoS_2.

KEYWORDS: *wafer-scale, monolayer molybdenum disulfide, oriented, large domain sizes, high quality*

Downloaded via INST OF PHYSICS on September 21, 2020 at 03:28:35 (UTC).
See https://pubs.acs.org/sharingguidelines for options on how to legitimately share published articles.

2H-phase monolayer molybdenum disulfide (ML-MoS_2) is a two-dimensional semiconductor with great potential for electronics and optoelectronics.[1−5] The controllable growth of wafer-scale uniform and high-quality continuous ML-MoS_2 is highly demanded to realize its full potential for these applications.[6−9] To date, to obtain wafer-scale high-quality ML-MoS_2 film, various approaches have been developed, including metal−organic chemical vapor deposition (MOCVD),[6] atomic layer deposition (ALD),[10] chemical vapor deposition (CVD),[11] etc. Among these methods, CVD shows great potential in growing MoS_2 with high quality.[12,13] The uniformity of the wafer-scale films is important when used in large-scale integrated circuits. However, spatial inhomogeneity over a large scale due to the nonuniform distribution of the source concentration in the vapor phase hinders the practical applications of the films.[14,15]

Domain boundaries in MoS_2 monolayers could degrade their electronic quality due to scattering effects.[16−19] To achieve better materials, one should align and enlarge domains in ML-MoS_2 films as much as possible. Recently, significant progress has been made along this direction by choosing appropriate substrates and optimizing the growth process.[11,16,20,21] By employing a high-temperature growth on sapphire substrates, we were able to achieve 2 in. wafer-scale bicrystalline ML-MoS_2 films with ∼1 μm domain sizes.[11] Centimeter-scale ML-MoS_2 films with 98% domains aligned in the same direction on gold substrates.[21] For the domain size control, the domain size can also be enlarged up to tens or even hundreds of microns in ML-MoS_2 films with random domain orientations.[12,13,22] However, high-quality ML-MoS_2 films with domain sizes exceeding 100 μm are still unavailable.

In this work, we report the success of the epitaxy of highly oriented and large-domain ML-MoS_2 films at a 4 in. wafer scale via a facile multisource CVD growth method. Almost only 0 and 60° oriented domains are present in films, and the domain size, on average, is greater than 180 μm at the largest. Although 4|4E-types of domain boundaries exist, they have no obvious impact on their overall electronic properties at room temperature. Our imaging, spectroscopy, and transport measurements of these ML-MoS_2 films suggest their best quality ever obtained, as evidenced from their wafer-scale homogeneity, nearly perfect lattice structure, and intrinsically high electronic quality (in terms of their field-effect on/off ratios, mobilities, and threshold voltages).

The epitaxial growth was performed in a specially designed 4 in. CVD system (Figure 1a and Figure S1). In this setup, seven miniature quartz tubes in the growth chamber served as pockets for reaction sources, and carrier gases through them are

Received: June 18, 2020
Revised: August 24, 2020
Published: August 24, 2020

© XXXX American Chemical Society

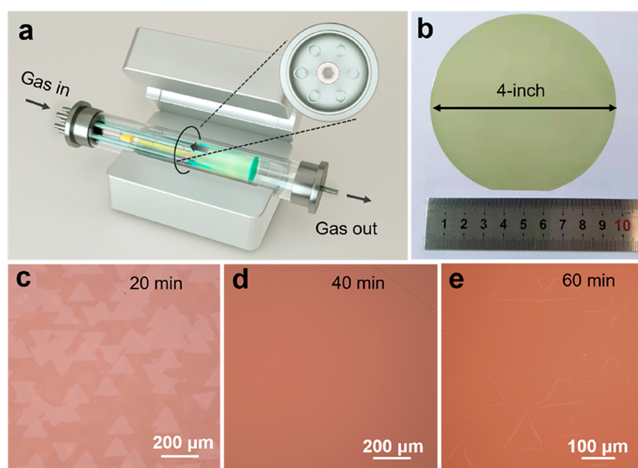

Figure 1. Growth of monolayer MoS_2 4 in. wafers. (a) Schematic diagram of the multisource CVD setup. (b) Photograph of a 4 in. sapphire wafer uniformly covered by monolayer MoS_2 film. (c−e) Optical images of MoS_2 grown on sapphire for different times with an O_2 flow rate of ∼10 sccm. The top right corner in (d) is an intentional scratch.

independently delivered. As seen in the inset of Figure 1a, MoO_3 sources are evenly loaded within the six minitubes, and the S source is loaded within the center minitube. The carrier gases for S and MoO_3 sources are Ar and Ar/O_2, respectively. This multisource design provides the homogeneous cross-sectional source supply, which is a key to uniform growth at the 4 in. wafer scale. During the growth, temperatures of the S source, MoO_3 sources, and sapphire wafers are 120, 540, and 930 °C, respectively. Note that 4 in. sapphire wafers were vertically placed in the growth chamber to avoid source concentration inhomogeneity along the horizontal direction. Benefiting from this multisource design, we can reliably grow a uniform MoS_2 monolayer epitaxially over the entire 4 in. wafer.

During the growth, Ar/O_2 carrier gases protect the MoO_3 sources from sulfurization, thus ensuring a steady evaporation. In addition, it can also balance the domain nucleation, growth, and etching.[23] Thus, domain sizes could be tuned by the O_2 flux; the more O_2 flows, the less domain nucleates. Of course, too much O_2 would stop the growth via etching, and it is a matter of trade off. Figure S2 shows the optical microscope images of ML-MoS_2 grown on sapphire for 20 min by employing different O_2 flow rates. When the O_2 flow rates are varied from 0 to 10 sccm, the domain size, on average, increases from ∼1 to ∼180 μm. When the oxygen flow rate is greater than 10 sccm, the domain size decreases gradually and it will be very difficult to form continuous films. We have further studied the temperature effect on the grain sizes. When the oxygen flow rate was kept at 10 sccm, the growth temperature varied from 800 to 1000 °C. At a low temperature of 800 °C, we usually get poor growth, for example, with small domain sizes and the presence of additional second layers. When the growth temperature increases from 870 to 1000 °C, the domain size, on average, decreases from ∼400 to ∼40 μm. Such domain size reduction comes from the oxygen etching effect (Figure S3). Note that when the temperature is less than 930 °C, the domain orientation control is not good. Considering both the domain alignment and domain size, we chose the optimized growth temperature of 930 °C and oxygen flow rate of 10 sccm. Extending the growth leads to merging of these domains into a continuous ML-MoS_2 film. Note that these domains in our sample are highly oriented, and we can clearly see almost only two domain orientations, that is, 0 and 60° relative to the underneath sapphire substrate, which is consistent with our previous observations on the 2 in. ML-MoS_2.[11] Note that the 4 in. sapphire wafer was vertically placed, whereas the substrate was horizontally placed in our previous 2 in. CVD growth chamber. In this new setup, substrates directly face the sources and can have a much higher growth speed. As a result, a great improvement of domain size in the present ML-MoS_2 can be achieved. Figure 1b shows an as-grown 4 in. wafer of fully covered ML-MoS_2 on sapphire with the average domain size exceeding 100 μm. Figure 1c−e shows the merging process of these highly oriented domains. When the growth time after the formation of a continuous monolayer film was increased further, a second layer MoS_2 will appear and prefer to seed above those domain boundaries (DBs) in the first layer (Figure 1e and Figure S4).[17] In this way, we can visualize the domain size and DB locations.

Figure 2a shows a typical atomic force microscope (AFM) image of the ML-MoS_2 film, and the height profile across a scratched trench on the surface (Figure S5) confirms the monolayer thickness of ∼0.7 nm. Images of a ML-MoS_2 wafer taken from different areas are shown in Figure S6. An ultraclean and atomically flat surface with a 4 in. wafer-scale uniformity can be visualized. Contaminations or a second layer are barely seen. We also imaged as-grown samples with a fluorescence microscope (Figure 2b). The uniform color contrast further confirms the optical uniformity of the ML-MoS_2. An aberration-corrected scanning transmission electron microscope (STEM), equipped with a high-angle annular dark-field detector (HAADF), was used to characterize the atomic structure of as-grown samples. Figure 2c shows an atomic structure of 60° domain boundaries in the obtained ML-MoS_2. This very straight boundary is a nearly perfect 4|4E type without vacancies and distortions (Figure 2d). According to previous studies, this type of boundary may show perfect metallicity.[24] A typical HAADF image and selected area electron diffraction (SAED) pattern inside a domain are shown in Figure 2e,f, respectively; we can see the nearly perfect honeycomb lattice of MoS_2. We further evaluated the chemical composition of our achieved MoS_2 films

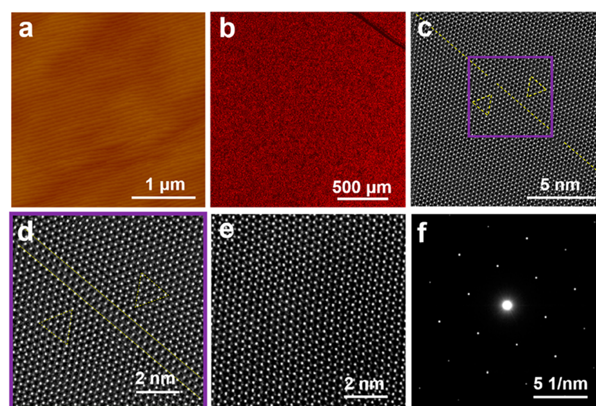

Figure 2. Structural characterizations of monolyer MoS_2 films. (a) AFM images of monolayer MoS_2 films (the step structure is from the underlying sapphire surface). (b) Fluorescence microscope image of the as-grown film with an intentional scratch on the upper right corner. (c) Typical STEM images of the MoS_2 domain boundary, and (d) zoomed-in image of the rectangular area in (c). (e) Typical STEM images within a grain. (f) SAED pattern of monolayer film.

https://dx.doi.org/10.1021/acs.nanolett.0c02531
Nano Lett. XXXX, XXX, XXX−XXX

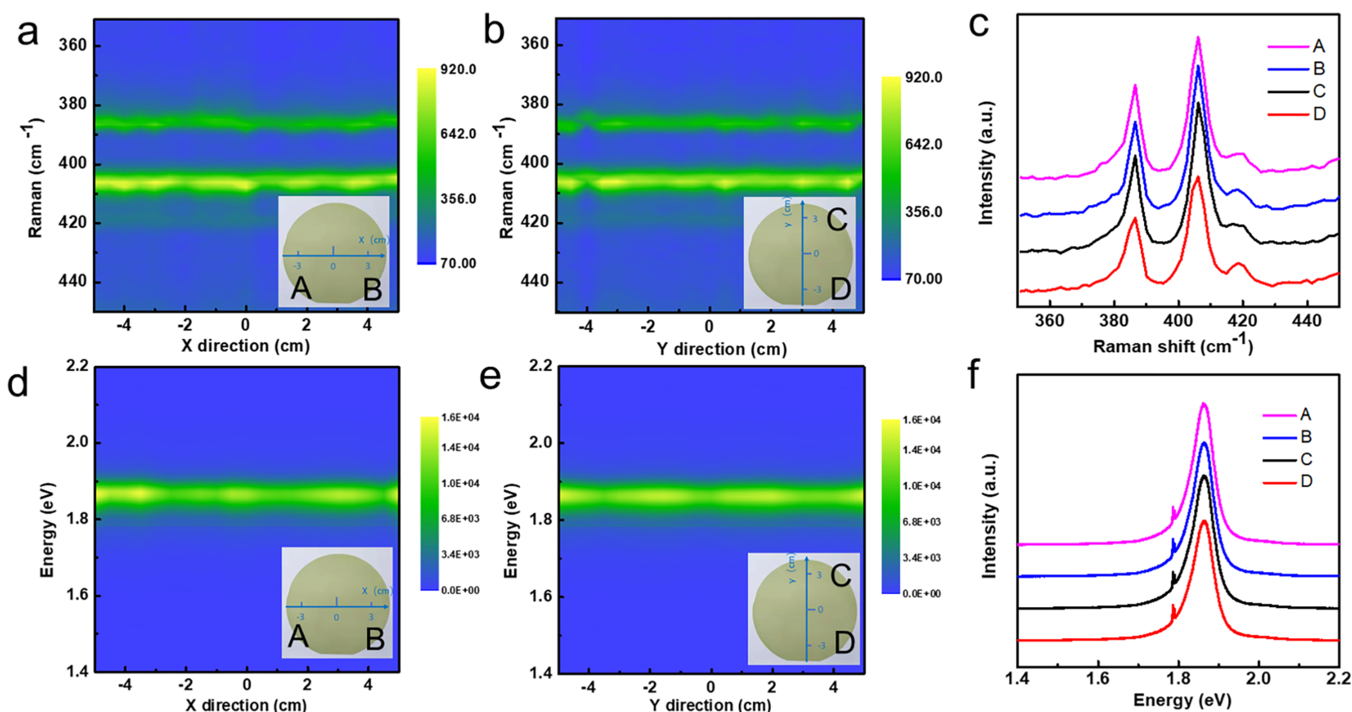

Figure 3. Wafer-scale uniformity of the synthesized MoS_2 monolayer. (a,b,d,e) Color-coded images of the typical Raman/PL line scan mapping along the diameter. (c,f) Corresponding Raman/PL spectra at four randomly picked locations on the wafer.

by X-ray photoelectron spectroscopy, and a low oxygen concentration (∼5%) was detected (Figure S7).

We also performed Raman and photoluminescence (PL) line scans across the entire 4 in. wafer of ML-MoS_2 on sapphire. Typical Raman/PL mapping results along the *X*- and *Y*-directions are shown in Figure 3a,d and b,e, respectively. Spectra at different locations are nearly the same, revealing a wafer-scale uniformity. Four representative Raman/PL spectra are shown in Figure 3c,f. Raman E_{2g} and A_{1g} peaks are located at 384 and 403 cm^{-1} with a full width at half-maximum of 4.8 and 6.8 cm^{-1}, respectively. The peak distance between E_{2g} and A_{1g} is 19 cm^{-1}, confirming the monolayer nature of the as-grown films.[25] We also characterized our as-grown sample by Raman spectroscopy and compared it with the exfoliated monolayer MoS_2 on SiO_2, and we did not observe a clear shift or split subpeaks in the Raman spectrum (Figure S8); this means the strain in our sample is small (less than 0.2%) possibly due to the relatively weak van der Waals interaction between MoS_2 and the sapphire substrate. PL spectra of the MoS_2 films show a single sharp excitonic A peak at ∼1.88 eV. Its narrow full width at half-maximum (i.e., ∼56 meV) also indicates very high crystalline quality. Also note that the statistical Raman peak distance between E_{2g} and A_{1g} is 19.7 ± 0.3 cm^{-1} from Figure 3a,b, indicating the superior monolayer thickness uniformity of the 4 in. wafer-scale ML-MoS_2 on sapphire.

In contrast to the previously reported wafer-scale ML-MoS_2 continuous films, these highly oriented and large domain samples should have improved electronic quality. To make a simple comparison, we thus transferred our films on 300 nm thick SiO_2/Si substrates and fabricated back-gated field-effect transistors (FETs). Figure S9 shows a batch production of 22 500 devices. Output and transfer curves of a typical device with channel length/width (*L*/*W*) of 10/25 μm are shown in Figure 4a,b, respectively. This device presents a high carrier mobility of 82 $cm^2 V^{-1} s^{-1}$, low off current of ∼15 fA, high on/off ratio of $\sim 2 \times 10^{10}$, and threshold voltage of 0 V, suggesting an excellent device performance. The velocity saturation occurs under a relatively high bias voltage (V_{ds}) as our FETs are in the long-channel regime.[8] The saturated current is about 1.22 mA, and the saturated current density (I_{ds}/W) can reach ∼49 μA/μm for a channel length of 10 μm (Figure S10). We measured 100 randomly picked devices in the batch, and the statistical data are shown in Figure 4c,d and Figure S9d. We can see that the device mobility averages to 70 $cm^2 V^{-1} s^{-1}$, and the highest mobility can reach 93 $cm^2 V^{-1} s^{-1}$. The average mobility of 70 $cm^2 V^{-1} s^{-1}$ is just slightly smaller than the number achieved for single-crystal samples (averages at 78 $cm^2 V^{-1} s^{-1}$, Figure S11), suggesting that the domain boundary densities in the present films are really low and that these twin domain boundaries have weak effects on electrical properties.[14] Note that the achieved devices' I_{on}/I_{off} ratio is much higher than those achieved in previous CVD MoS_2;[12,21,22,26−28] to our best knowledge, the present ML-MoS_2 films have the highest electrical quality (Figure 4e and Table S1).[6,9,11,12,21,22,27−30] The threshold voltage value is mainly located at 0−5 V (Figure S9d). We also fabricated inverter, NAND, NOR, and AND gate devices based on such films. The voltage transfer curves of the inverter is plotted in Figure 4f. In this inverter, a sharp voltage switching is realized, and a high voltage gain of 90 is achieved at the drive voltages of 5 V. Furthermore, the logic function can successfully be achieved in our devices (Figure 4g−i), which means the obtained films have great potential for integrated circuits. We also performed the growth of MoS_2 directly on SiO_2/Si, which is a universal substrate for semiconductor processes (Figure S13). The domain size (∼5 μm) is smaller than those on sapphire due to the relatively high surface roughness of SiO_2. The amorphous nature of SiO_2 also leads to a random orientation of MoS_2 domains. We characterized the electrical properties of achieved films on the SiO_2/Si substrate, and the FET devices present a carrier mobility of ∼35 $cm^2 V^{-1} s^{-1}$ and an on/off ratio of $\sim 10^8$.

https://dx.doi.org/10.1021/acs.nanolett.0c02531
Nano Lett. XXXX, XXX, XXX−XXX

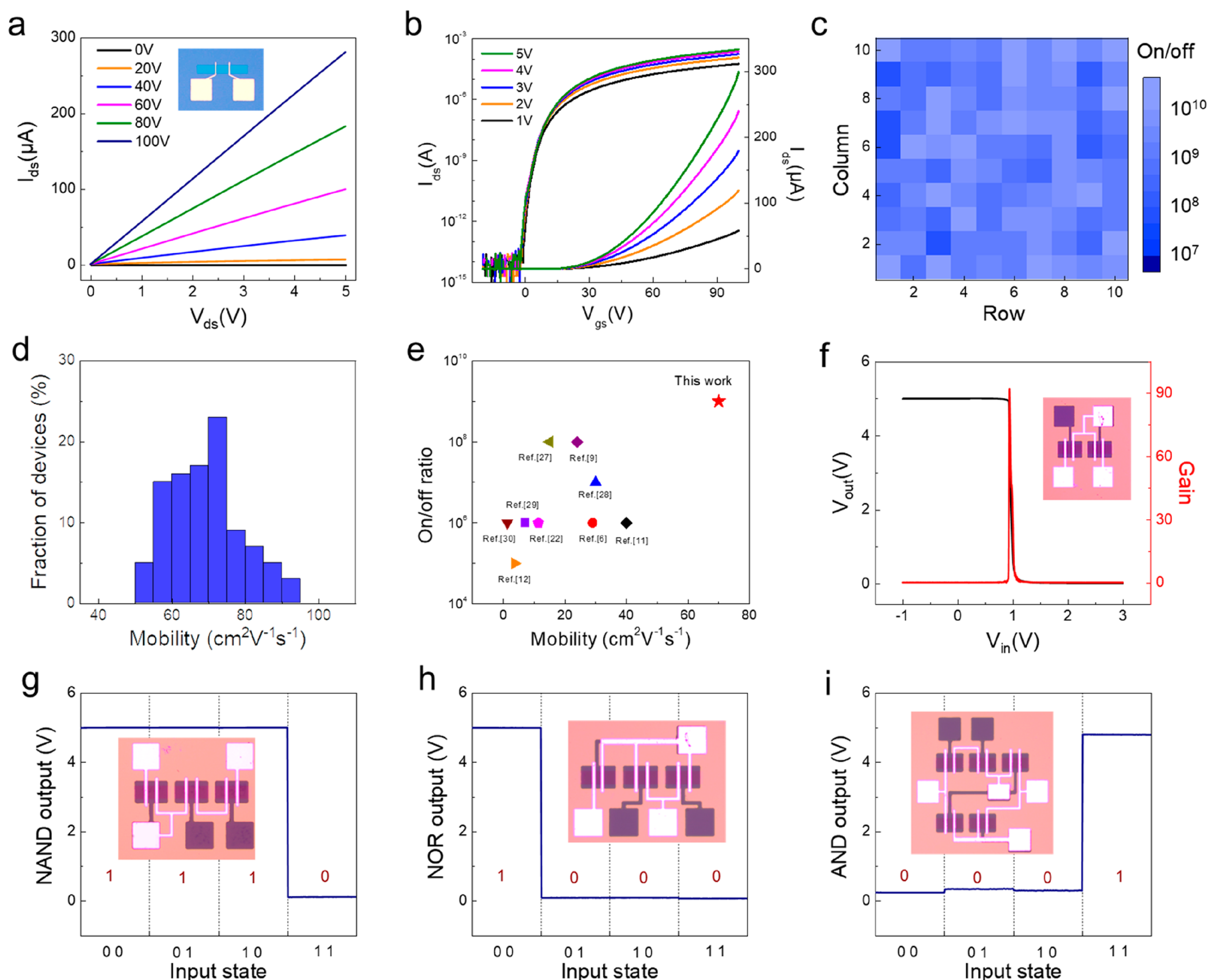

Figure 4. Transport properties and logic gates of as-grown monolayer MoS_2 films. (a,b) Output/tranfer curves of a typical FET. The on/off ratio (c) and mobility (d) of 100 random MoS_2 FETs. (e) Comparison of MoS_2 electrical performance at room temperature. (f) Voltage transfer characteristic of an inverter (left axis) and the corresponding voltage gain of the transfer curve (right axis). (g–i) Output characteristics of NAND (g), NOR (h), and AND (i) gates.

This performance is worse than that of our highly oriented MoS_2 monolayers with large domain sizes.

In summary, we report the realization of 4 in. wafer-scale expitaxy of highly oriented MoS_2 monolayers with large domain sizes. Benefiting from a multisource design in a CVD process, as-grown MoS_2 monolayers on sapphire show remarkable uniformity across the entire wafers. Domain sizes, orientations, and boundaries in these monolayer films were visualized by optical, scanning probe, and transmission electron microscopes. Nearly perfect 4|4E types of domain boundaries were observed but do not contribute significantly to their field-effect properties. We fabricated FETs based on these produced monolayers and achieved an average room-temperature device mobility of ~70 cm^2 V^{-1} s^{-1} and an on/off ratio of $\sim 10^9$ on SiO_2. High-performance logic inverters, NOR, NAND, and AND gates were also demonstrated. Our electronic and spectroscopic characterizations suggest that the produced ML-MoS_2 4 in. wafers are of the highest electronic quality so far and ready for use for many fascinating applications.

METHODS

CVD Growth of MoS_2 on Sapphire. The multisource CVD system was manufactured by Dongguan Join Technology Co., Ltd. For a typical growth, the center miniature quartz tube was loaded with S (Alfa Aesar, 99.9%, 8 g) and flowed with Ar (40 sccm), and the outside six miniature quartz tubes were individually loaded with MoO_3 (Alfa Aesar, 99.999%, 30 mg) and flowed with Ar/O_2 (240/10 sccm). Sapphire wafers were annealed in an oxygen atmosphere at 1000 °C for 4 h prior to the growth to form an atomically flat surface for subsequent MoS_2 growth. A typical growth lasts for ~40 min, and the pressure in the growth chamber is ~1 Torr.

Structural and Spectroscopic Characterizations. AFM imaging was performed by Asylum Research Cypher S. PL and Raman characterizations were performed with a Horiba Jobin Yvon LabRAM HR-Evolution Raman system with an excitation laser wavelength of 532 nm and a laser power of 1 mW. SAED was performed with a TEM (Philips CM200) operating at 200 kV, whereas high-resolution TEM was performed with an

https://dx.doi.org/10.1021/acs.nanolett.0c02531
Nano Lett. XXXX, XXX, XXX−XXX

aberration-corrected scanning transmission electron microscope JEM ARM200F (JEOL) operating at 200 kV.

Device Fabrication and Measurements. ML-MoS_2 films were etched off substrates in KOH solution and transferred onto SiO_2/Si substrates. The transferred 4 in. wafer-scale ML-MoS_2 was then patterned into FETs by UV lithography (MA6, Karl Suss), oxygen plasma etching (RIE, Plasma Lab 80 Plus, Oxford Instruments Company), electron beam evaporation, and lifting-off processes. The contact electrodes are Au/Ti/Au (2/2/30 nm). Electrical measurements were carried out with a semiconductor parameter analyzer (Agilent 4156C) in a four-probe vacuum station with a bass pressure of $\sim 10^{-6}$ mbar.

■ ASSOCIATED CONTENT

Supporting Information

The Supporting Information is available free of charge at https://pubs.acs.org/doi/10.1021/acs.nanolett.0c02531.

Photo of the 4 in. multisource CVD system, more growth results under different oxygen flux and temperature, AFM and STEM images of additional layer growth on grain boundaries, AFM images of different locations of a wafer, XPS and Raman characterizations to confirm the oxygen concentration and strain in MoS_2 films, more electrical measurements for MoS_2 films, detailed structure of logic circuits and the MoS_2 growth results on SiO_2/Si substrates (PDF)

■ AUTHOR INFORMATION

Corresponding Author

Guangyu Zhang − *Beijing National Laboratory for Condensed Matter Physics, Key Laboratory for Nanoscale Physics and Devices, Institute of Physics, Chinese Academy of Sciences, Beijing 100190, China; School of Physical Sciences, University of Chinese Academy of Sciences, Beijing 100190, China; Beijing Key Laboratory for Nanomaterials and Nanodevices, Beijing 100190, China; Songshan Lake Materials Laboratory, Dongguan, Guangdong 523808, China*; Email: gyzhang@iphy.ac.cn

Authors

Qinqin Wang − *Beijing National Laboratory for Condensed Matter Physics, Key Laboratory for Nanoscale Physics and Devices, Institute of Physics, Chinese Academy of Sciences, Beijing 100190, China; School of Physical Sciences, University of Chinese Academy of Sciences, Beijing 100190, China*

Na Li − *Beijing National Laboratory for Condensed Matter Physics, Key Laboratory for Nanoscale Physics and Devices, Institute of Physics, Chinese Academy of Sciences, Beijing 100190, China; School of Physical Sciences, University of Chinese Academy of Sciences, Beijing 100190, China*

Jian Tang − *Beijing National Laboratory for Condensed Matter Physics, Key Laboratory for Nanoscale Physics and Devices, Institute of Physics, Chinese Academy of Sciences, Beijing 100190, China; School of Physical Sciences, University of Chinese Academy of Sciences, Beijing 100190, China*

Jianqi Zhu − *Beijing National Laboratory for Condensed Matter Physics, Key Laboratory for Nanoscale Physics and Devices, Institute of Physics, Chinese Academy of Sciences, Beijing 100190, China; School of Physical Sciences, University of Chinese Academy of Sciences, Beijing 100190, China*

Qinghua Zhang − *Beijing National Laboratory for Condensed Matter Physics, Key Laboratory for Nanoscale Physics and Devices, Institute of Physics, Chinese Academy of Sciences, Beijing 100190, China; School of Physical Sciences, University of Chinese Academy of Sciences, Beijing 100190, China*

Qi Jia − *Beijing National Laboratory for Condensed Matter Physics, Key Laboratory for Nanoscale Physics and Devices, Institute of Physics, Chinese Academy of Sciences, Beijing 100190, China; School of Physical Sciences, University of Chinese Academy of Sciences, Beijing 100190, China*

Ying Lu − *Beijing National Laboratory for Condensed Matter Physics, Key Laboratory for Nanoscale Physics and Devices, Institute of Physics, Chinese Academy of Sciences, Beijing 100190, China; School of Physical Sciences, University of Chinese Academy of Sciences, Beijing 100190, China*; orcid.org/0000-0002-8421-7228

Zheng Wei − *Beijing National Laboratory for Condensed Matter Physics, Key Laboratory for Nanoscale Physics and Devices, Institute of Physics, Chinese Academy of Sciences, Beijing 100190, China; School of Physical Sciences, University of Chinese Academy of Sciences, Beijing 100190, China*

Hua Yu − *Beijing National Laboratory for Condensed Matter Physics, Key Laboratory for Nanoscale Physics and Devices, Institute of Physics, Chinese Academy of Sciences, Beijing 100190, China; School of Physical Sciences, University of Chinese Academy of Sciences, Beijing 100190, China*

Yanchong Zhao − *Beijing National Laboratory for Condensed Matter Physics, Key Laboratory for Nanoscale Physics and Devices, Institute of Physics, Chinese Academy of Sciences, Beijing 100190, China; School of Physical Sciences, University of Chinese Academy of Sciences, Beijing 100190, China*

Yutuo Guo − *Beijing National Laboratory for Condensed Matter Physics, Key Laboratory for Nanoscale Physics and Devices, Institute of Physics, Chinese Academy of Sciences, Beijing 100190, China; School of Physical Sciences, University of Chinese Academy of Sciences, Beijing 100190, China*

Lin Gu − *Beijing National Laboratory for Condensed Matter Physics, Key Laboratory for Nanoscale Physics and Devices, Institute of Physics, Chinese Academy of Sciences, Beijing 100190, China; School of Physical Sciences, University of Chinese Academy of Sciences, Beijing 100190, China*; orcid.org/0000-0002-7504-031X

Gang Sun − *Beijing National Laboratory for Condensed Matter Physics, Key Laboratory for Nanoscale Physics and Devices, Institute of Physics, Chinese Academy of Sciences, Beijing 100190, China; School of Physical Sciences, University of Chinese Academy of Sciences, Beijing 100190, China*

Wei Yang − *Beijing National Laboratory for Condensed Matter Physics, Key Laboratory for Nanoscale Physics and Devices, Institute of Physics, Chinese Academy of Sciences, Beijing 100190, China; School of Physical Sciences, University of Chinese Academy of Sciences, Beijing 100190, China; Beijing Key Laboratory for Nanomaterials and Nanodevices, Beijing 100190, China*

Rong Yang − *Beijing National Laboratory for Condensed Matter Physics, Key Laboratory for Nanoscale Physics and Devices, Institute of Physics, Chinese Academy of Sciences, Beijing 100190, China; Beijing Key Laboratory for Nanomaterials and Nanodevices, Beijing 100190, China; Songshan Lake Materials Laboratory, Dongguan, Guangdong 523808, China*; orcid.org/0000-0001-5936-6849

Dongxia Shi − *Beijing National Laboratory for Condensed Matter Physics, Key Laboratory for Nanoscale Physics and Devices, Institute of Physics, Chinese Academy of Sciences, Beijing 100190, China; School of Physical Sciences, University of Chinese Academy of Sciences, Beijing 100190, China; Beijing Key*

Laboratory for Nanomaterials and Nanodevices, Beijing 100190, China

Complete contact information is available at:
https://pubs.acs.org/10.1021/acs.nanolett.0c02531

Author Contributions

G.Z. designed the research; Q.W. performed the epitaxial growth, device fabrications, and measurements. N.L. and J.T. helped with fabrication of the logic circuits. J.T., Q.Z., and L.G. performed TEM and structural analysis. Q.J. and Y.L. performed fluorescence microscopy measurements. Q.W. and G.Z. wrote and all authors commented on the manuscript.

Notes

The authors declare no competing financial interest.

ACKNOWLEDGMENTS

This work was supported by the National Science Foundation of China (NSFC) under Grant Nos. 11834017, 11574361, and 61888102, the Strategic Priority Research Program of Chinese Academy of Sciences (CAS) under Grant No. XDB30000000, the Key Research Program of Frontier Sciences of the CAS under Grant No. QYZDB-SSW-SLH004, the Youth Innovation Promotion Association CAS (No. 2018013), the National Key R&D program under Grant No. 2016YFA0300904, and the Research Program of Beijing Academy of Quantum Information Sciences under Grant No. Y18G11.

REFERENCES

(1) Lin, Z.; Liu, Y.; Halim, U.; Ding, M.; Liu, Y.; Wang, Y.; Jia, C.; Chen, P.; Duan, X.; Wang, C.; Song, F.; Li, M.; Wan, C.; Huang, Y.; Duan, X. Solution-Processable 2D Semiconductors for High-Performance Large-Area Electronics. *Nature* **2018**, *562*, 254−258.

(2) Wang, Q. H.; Kalantar-Zadeh, K.; Kis, A.; Coleman, J. N.; Strano, M. S. Electronics and Optoelectronics of Two-Dimensional Transition Metal Dichalcogenides. *Nat. Nanotechnol.* **2012**, *7*, 699−712.

(3) Desai, S. B.; Madhvapathy, S. R.; Sachid, A. B.; Llinas, J. P.; Wang, Q.; Ahn, G. H.; Pitner, G.; Kim, M. J.; Bokor, J.; Hu, C.; Wong, H. P.; Javey, A. MoS_2 Transistors with 1-nanometer Gate Lengths. *Science* **2016**, *354*, 99−102.

(4) Manzeli, S.; Ovchinnikov, D.; Pasquier, D.; Yazyev, O. V.; Kis, A. 2D Transition Metal Dichalcogenides. *Nat. Rev. Mater.* **2017**, *2*, 17033.

(5) Bhimanapati, G. R.; Lin, Z.; Meunier, V.; Jung, Y.; Cha, J.; Das, S.; Xiao, D.; Son, Y.; Strano, M. S.; Cooper, V. R.; Liang, L.; Louie, S. G.; Ringe, E.; Zhou, W.; Kim, S. S.; Naik, R. R.; Sumpter, B. G.; Terrones, H.; Xia, F.; Wang, Y.; Zhu, J.; Akinwande, D.; Alem, N.; Schuller, J. A.; Schaak, R. E.; Terrones, M.; Robinson, J. A. Recent Advances in Two-Dimensional Materials beyond Graphene. *ACS Nano* **2015**, *9*, 11509−11539.

(6) Kang, K.; Xie, S.; Huang, L.; Han, Y.; Huang, P. Y.; Mak, K. F.; Kim, C. J.; Muller, D.; Park, J. High-Mobility Three-Atom-Thick Semiconducting Films with Wafer-Scale Homogeneity. *Nature* **2015**, *520*, 656−660.

(7) Xu, X.; Das, G.; He, X.; Hedhili, M. N.; Fabrizio, E. D.; Zhang, X.; Alshareef, H. N. High-Performance Monolayer MoS_2 Films at the Wafer Scale by Two-Step Growth. *Adv. Funct. Mater.* **2019**, *29*, 1901070.

(8) Xu, H.; Zhang, H.; Guo, Z.; Shan, Y.; Wu, S.; Wang, J.; Hu, W.; Liu, H.; Sun, Z.; Luo, C.; Wu, X.; Xu, Z.; Zhang, D. W.; Bao, W.; Zhou, P. High-Performance Wafer-Scale MoS_2 Transistors toward Practical Application. *Small* **2018**, *14*, 1803465.

(9) Zhang, Z. F.; Xu, X. L.; Song, J.; Gao, Q. G.; Li, S. C.; Hu, Q. L.; Li, X. F.; Wu, Y. Q. High-Performance Transistors based on Monolayer CVD MoS_2 Grown on Molten Glass. *Appl. Phys. Lett.* **2018**, *113*, 202103.

(10) Pyeon, J. J.; Kim, S. H.; Jeong, D. S.; Baek, S. H.; Kang, C. Y.; Kim, J. S.; Kim, S. K. Wafer-Scale Growth of MoS_2 Thin Films by Atomic Layer Deposition. *Nanoscale* **2016**, *8*, 10792−10798.

(11) Yu, H.; Liao, M.; Zhao, W.; Liu, G.; Zhou, X. J.; Wei, Z.; Xu, X.; Liu, K.; Hu, Z.; Deng, K.; Zhou, S.; Shi, J. A.; Gu, L.; Shen, C.; Zhang, T.; Du, L.; Xie, L.; Zhu, J.; Chen, W.; Yang, R.; Shi, D.; Zhang, G. Wafer-Scale Growth and Transfer of Highly-Oriented Monolayer MoS_2 Continuous Films. *ACS Nano* **2017**, *11*, 12001−12007.

(12) Tao, L.; Chen, K.; Chen, Z.; Chen, W.; Gui, X.; Chen, H.; Li, X.; Xu, J. B. Centimeter-Scale CVD Growth of Highly Crystalline Single-Layer MoS_2 Film with Spatial Homogeneity and the Visualization of Grain Boundaries. *ACS Appl. Mater. Interfaces* **2017**, *9*, 12073−12081.

(13) Lim, Y. F.; Priyadarshi, K.; Bussolotti, F.; Gogoi, P. K.; Cui, X.; Yang, M.; Pan, J.; Tong, S. W.; Wang, S.; Pennycook, S. J.; Goh, K. E. J.; Wee, A. T. S.; Wong, S. L.; Chi, D. Modification of Vapor Phase Concentrations in MoS_2 Growth Using a NiO Foam Barrier. *ACS Nano* **2018**, *12*, 1339−1349.

(14) Van Der Zande, A. M.; Huang, P. Y.; Chenet, D. A.; Berkelbach, T. C.; You, Y.; Lee, G. H.; Heinz, T. F.; Reichman, D. R.; Muller, D. A.; Hone, J. C. Grains and Grain Boundaries in Highly Crystalline Monolayer Molybdenum Disulphide. *Nat. Mater.* **2013**, *12*, 554−561.

(15) Tang, L.; Li, T.; Luo, Y.; Feng, S.; Cai, Z.; Zhang, H.; Liu, B.; Cheng, H. M. Vertical Chemical Vapor Deposition Growth of Highly Uniform 2D Transition Metal Dichalcogenides. *ACS Nano* **2020**, *14*, 4646−4653.

(16) Dumcenco, D.; Ovchinnikov, D.; Marinov, K.; Lazic, P.; Gibertini, M.; Marzari, N.; Sanchez, O. L.; Kung, Y.-C.; Krasnozhon, D.; Chen, M.-W.; Bertolazzi, S.; Gillet, P.; Fontcuberta i Morral, A.; Radenovic, A.; Kis, A. Large-Area Epitaxial Monolayer MoS_2. *ACS Nano* **2015**, *9*, 4611−4620.

(17) Najmaei, S.; Amani, M.; Chin, M. L.; Liu, Z.; Birdwell, A. G.; O'Regan, T. P.; Ajayan, P. M.; Dubey, M.; Lou, J. Electrical Transport Properties of Polycrystalline Monolayer Molybdenum Disulfide. *ACS Nano* **2014**, *8*, 7930−7937.

(18) Cai, Z.; Liu, B.; Zou, X.; Cheng, H. M. Chemical Vapor Deposition Growth and Applications of Two-Dimensional Materials and Their Heterostructures. *Chem. Rev.* **2018**, *118*, 6091−6133.

(19) Tong, S. W.; Medina, H.; Liao, W.; Wu, J.; Wu, W.; Chai, J.; Yang, M.; Abutaha, A.; Wang, S.; Zhu, C.; Hippalgaonkar, K.; Chi, D. Employing a Bifunctional Molybdate Precursor To Grow the Highly Crystalline MoS_2 for High-Performance Field-Effect Transistors. *ACS Appl. Mater. Interfaces* **2019**, *11*, 14239−14248.

(20) Aljarb, A.; Cao, Z.; Tang, H. L.; Huang, J. K.; Li, M.; Hu, W.; Cavallo, L.; Li, L. J. Substrate Lattice-Guided Seed Formation Controls the Orientation of 2D Transition-Metal Dichalcogenides. *ACS Nano* **2017**, *11*, 9215−9222.

(21) Yang, P.; Zhang, S.; Pan, S.; Tang, B.; Liang, Y.; Zhao, X.; Zhang, Z.; Shi, J.; Huan, Y.; Shi, Y.; Pennycook, S. J.; Ren, Z.; Zhang, G.; Chen, Q.; Zou, X.; Liu, Z.; Zhang, Y. Epitaxial Growth of Centimeter-Scale Single-Crystal MoS_2 Monolayer on Au (111). *ACS Nano* **2020**, *14*, 5036−5045.

(22) Yang, P.; Zou, X.; Zhang, Z.; Hong, M.; Shi, J.; Chen, S.; Shu, J.; Zhao, L.; Jiang, S.; Zhou, X.; Huan, Y.; Xie, C.; Gao, P.; Chen, Q.; Zhang, Q.; Liu, Z.; Zhang, Y. Batch Production of 6-in. Uniform Monolayer Molybdenum Disulfide Catalyzed by Sodium in Glass. *Nat. Commun.* **2018**, *9*, 979.

(23) Chen, W.; Zhao, J.; Zhang, J.; Gu, L.; Yang, Z.; Li, X.; Yu, H.; Zhu, X.; Yang, R.; Shi, D.; Lin, X.; Guo, J.; Bai, X.; Zhang, G. Oxygen-Assisted Chemical Vapor Deposition Growth of Large Single-Crystal and High-Quality Monolayer MoS_2. *J. Am. Chem. Soc.* **2015**, *137*, 15632−15635.

(24) Zhou, W.; Zou, X.; Najmaei, S.; Liu, Z.; Shi, Y.; Kong, J.; Lou, J.; Ajayan, P. M.; Yakobson, B. I.; Idrobo, J. C. Intrinsic Structural Defects in Monolayer Molybdenum Disulfide. *Nano Lett.* **2013**, *13*, 2615−2622.

(25) Lee, C.; Yan, H.; Brus, L. E.; Heinz, T. F.; Hone, J.; Ryu, S. Anomalous Lattice Vibrations of Single- and Few-layer MoS_2. *ACS Nano* **2010**, *4*, 2695−2700.

(26) Zhao, M.; Ye, Y.; Han, Y.; Xia, Y.; Zhu, H.; Wang, S.; Wang, Y.; Muller, D. A.; Zhang, X. Large-Scale Chemical Assembly of Atomically Thin Transistors and Circuits. *Nat. Nanotechnol.* **2016**, *11*, 954.
(27) Ju, M.; Liang, X.; Liu, J.; Zhou, L.; Liu, Z.; Mendes, R. G.; Rümmeli, M. H.; Fu, L. Universal Substrate-Trapping Strategy To Grow Strictly Monolayer Transition Metal Dichalcogenides Crystals. *Chem. Mater.* **2017**, *29*, 6095−6103.
(28) Zhu, J.; Xu, H.; Zou, G.; Zhang, W.; Chai, R.; Choi, J.; Wu, J.; Liu, H.; Shen, G.; Fan, H. MoS_2-OH Bilayer-Mediated Growth of Inch-Sized Monolayer MoS_2 on Arbitrary Substrates. *J. Am. Chem. Soc.* **2019**, *141*, 5392−5401.
(29) Zhang, J.; Yu, H.; Chen, W.; Tian, X.; Liu, D.; Cheng, M.; Xie, G.; Yang, W.; Yang, R.; Bai, X.; Shi, D.; Zhang, G. Scalable Growth of High-Quality Polycrystalline MoS_2 Monolayers on SiO_2 with Tunable Grain Sizes. *ACS Nano* **2014**, *8*, 6024−6030.
(30) Song, X.; Zan, W.; Xu, H.; Ding, S.; Zhou, P.; Bao, W.; Zhang, D. W. A Novel Synthesis Method for Large-Area MoS_2 Film with Improved Electrical Contact. *2D Mater.* **2017**, *4*, 025051.

https://dx.doi.org/10.1021/acs.nanolett.0c02531
Nano Lett. XXXX, XXX, XXX−XXX